A novel micro-ECoG recording method for recording multisensory neural activity from the parietal to temporal cortices in mice

Susumu Setogawa[1,2], Ryota Kanda[3], Shuto Tada[3], Yoshito Saitoh[1], Mikiko Ishikawa[1], Satoshi Nakada[4], Fumiko Seki[5], Keigo Hikishima[6], Hideyuki Matsumoto[2], Kenji Mizuseki[2], Osamu Fukayama[7], Makoto Osanai[8], Hiroto Sekiguchi[3,9,*], and Noriaki Ohkawa[1,*]

[1] Division for Memory and Cognitive Function, Research Center for Advanced Medical Science, Comprehensive Research Facilities for Advanced Medical Science, Dokkyo Medical University, Tochigi 321-0293, Japan

[2] Department of Physiology, Osaka Metropolitan University Graduate School of Medicine, Osaka 545-8585, Japan

[3] Department of Electrical and Electronic Information Engineering, Toyohashi University of Technology, Toyohashi, Aichi 441-8580, Japan

[4] Japanese Center for Research on Women in Sport, Juntendo University Graduate School of Health and Sports Science, Chiba 270-1695, Japan.

[5] Live Animal Imaging Center, Central Institutes for Experimental Animals (CIEA), Kanagawa 210-0821, Japan

[6] Medical Devices Research Group, Health and Medical Research Institute, National Institute of Advanced Industrial Science and Technology (AIST), Tsukuba 305-8564, Japan.

[7] Information and Neural Networks Lab, Center for Information and Neural Networks (CiNet), National Institute of Information and Communications Technology, Suita, Osaka 565-0871, Japan

[8] Laboratory for Physiological Functional Imaging, Department of Medical Physics and Engineering, Division of Health Sciences, Osaka University Graduate School of Medicine, Suita, Osaka 565-0871, Japan

[9] Japan Science and Technology, Precursory Research for Embryonic Science and Technology (PRESTO), Kawaguchi, Saitama 332-0012, Japan.

*Address for correspondence:

Noriaki Ohkawa, Ph.D

Division for Memory and Cognitive Function, Research Center for Advanced Medical Science, Comprehensive Research Facilities for Advanced Medical Science, Dokkyo Medical University, Tochigi 321-0293, Japan

E-mail: nohkawa@dokkyomed.ac.jp

Tell: +81-6-6645-3717

Hiroto Sekiguchi, Ph.D

Department of Electrical and Electronic Information Engineering, Toyohashi University of Technology, Toyohashi, Aichi 441-8580, Japan

E-mail: sekiguchi@ee.tut.ac.jp

Tell: +81-532-44-6744

Highlights

- A 64-channel parylene-based micro-ECoG allows access to the mouse temporal cortex.
- Thickness, width, and metal wiring determined bending stiffness of micro-ECoG sheets.
- Micro-ECoG enables the large-scale recordings without structural damage to cortical surface.
- Somatosensory and odor stimulus-evoked activities were recorded simultaneously.

Abstract

Background

Characterization of inter-regional interactions in brain is essential for understanding the mechanism relevant to normal brain function and neurological disease. The recently developed flexible micro (μ)-electrocorticography (μECoG) device is one prominent method used to examine large-scale cortical activity across multiple regions. The sheet-shaped μECoG electrodes arrays can be placed on a relatively wide area of cortical surface beneath the skull by inserting the device into the space between skull and brain. Although rats and mice are useful tools for neuroscience, current μECoG recording methods in these animals are limited to the parietal region of cerebral cortex. Recording cortical activity from the temporal region of cortex in mice has proven difficult because of surgical barriers created by the skull and surrounding temporalis muscle anatomy.

New method

Hear, we developed a sheet-shaped 64-channel μECoG device that allows access to the mouse temporal cortex, and we determined the factor determining the appropriate bending stiffness for the μECoG electrode array. We also established a surgical technique to implant the electrode arrays into the epidural space over a wide area of cerebral cortex covering from the barrel field to olfactory (piriform) cortex, which is the deepest region of the cerebral cortex.

Results

Using histology and computed tomography (CT) images, we confirmed that the tip of the μECoG device reached to the most ventral part of cerebral cortex without causing noticeable damage to the brain surface. The device simultaneously recorded somatosensory and odor stimulus-evoked neural activity from dorsal and ventral parts of cerebral cortex in awake and anesthetized mice.

Conclusions

These data indicates that our μECoG device and surgical techniques enable to record large-scale cortical activity from the parietal to temporal cortex in mice, including somatosensory and olfactory cortices. This system will provide opportunities to investigate physiological functions from wider areas of the mouse cerebral cortex than those of existing ECoG techniques.

Key Words

Electrocorticography, flexible micro-electrocorticography device, Multi-sensory, Cerebral cortex, Temporal cortex, Local Field Potential

Abbreviations: micro (m)-electrocorticography (mECoG), computed tomography (CT), electroencephalography (EEG), local field potential (LFP), printed circuit board (PCB), 4',6-diamidino-2-phenylindole (DAPI)

1. Introduction

Neural networks in the cerebral cortex are composed of functionally different regions which process information from distinct modalities to drive cognitive functions including attention, learning, and memory. Altered network activity from multiple cortical regions is linked to neurological disorders, such as seizure, dementia, and schizophrenia (Kramer and Cash, 2012; Li et al., 2019; Uhlhaas and Singer, 2010). Therefore, characterization of inter-cortical interactions is essential for understanding the mechanisms underlying normal cognitive functions and neuropathology.

Methods in neuroscience, such as large-scale calcium imaging, electroencephalography (EEG), and electrocorticography (ECoG), enable the monitoring of neural activity from a wide area of cerebral cortex, providing insight into inter-regional cortical network interactions (Choi et al., 2010; Gilad and Helmchen, 2020; Khodagholy et al., 2015). These techniques, combined with rodent experiments and a variety of genetic tools, have contributed to advances in neuroscience (Vázquez-Guardado et al., 2020). However, the measurement area of current large-scale calcium imaging and electrophysiological techniques focusing on cerebral cortex has been mostly limited to parietal regions, including sensorimotor, visual, auditory, parietal, and retrosplenial cortices (Gilad and Helmchen, 2020; Khodagholy et al., 2017; Sheybani et al., 2018). A major reason for the limitation in measurement area is the difficulty in the associated operation, since the temporal region of the cortex is covered by skull surrounded with temporalis muscles (Baverstock et al., 2013). Moreover, the most

common methods that use head fixation in rats and mice, such as the ear bars used in craniotomy and the head-fixation plate (Kimura et al., 2012), interferes with microscopy and electrode implantation for large-scale recordings of the temporal cortex. Given that the temporal cortex in rodents, including the piriform, insular, and entorhinal cortex, is involved in various types of cognitive processes (Lee et al., 2021; Rogers-Carter et al., 2018; Wang et al., 2019), establishing large-scale recording techniques covering the parietal to temporal parts of cortices would increase understanding of network dynamics underlying normal cognitive functions and their disruption in diseases.

The μECoG device with high-density multi-channel electrodes, which is fabricated by semiconductor technology, enables us to simultaneously record local field potentials (LFPs) from multiple regions in cerebral cortex with high spatiotemporal resolution (Kaiju et al., 2017; Konerding et al., 2018; Yeager et al., 2008). The sheet-shaped μECoG device which has been developed using parylene C to reduce sheet thickness, has improved electrode adhesiveness to the curved surface of the brain (Khodagholy et al., 2015). Thinning of the sheet-shaped electrodes reduces stiffness and enhances electrode contact to the subject (Park et al., 2016). It has been shown that a relatively thick sheet of μECoG electrode array can be implanted into the cerebral cortex through a small slit on the parietal bone (Park et al., 2016; Yeager et al., 2008). The electrode arrays make good contact with the brain surface due to compression pressure between the brain and skull, despite adopting the relatively thick sheet in the electrode array. Previous experiments have improved μECoG techniques in order to

mitigate anatomical and environmental factors that hinder electrophysiology recordings from cortical regions. Whereas μECoG techniques have the potential to provide a more large-scale neural recording system, a method that covers the parietal and temporal cortex in rodent models has not been developed.

The goal of this study is to develop a sheet-shaped μECoG device that is implantable into the epidural space, and to establish the optimal surgical procedures to record from the multisensory regions in temporal cortex. From calculations on the bending stiffness of the μECoG sheet, we showed that the thickness, width, and channel number of metal wiring are key factors for developing μECoG parylene-based electrode arrays. These arrays can be inserted into the space between the skull and brain for optimal large-scale neural recording. After surgical insertion of the sheet-shaped μECoG device, we used histological methods and CT images to confirm that the position of the sheet tip reached to the most ventral part of cerebral cortex without structural damage to the brain surface. This μECoG device allowed successive LFP recordings along the dorsoventral arc of cerebral cortex in an awake mouse. In addition, we simultaneously recorded neural responses corresponding to somatosensory and odor stimuli from different electrodes placed on the parietal and temporal cortex in anesthetized mice. These results show that the sheet-shaped μECoG permits acquisition of large-scale LFP recordings from the parietal to temporal cortex in mice, including somatosensory and olfactory areas.

2. Materials and methods

2.1. Device fabrication

The neural electrode array was fabricated on biocompatible parylene film using a standard semiconductor process (Fig. 1a). First, a thick parylene film was deposited as a base layer on a Si substrate using a parylene coater (PDS2010, Specialty Coating Systems Inc.). Subsequently, a Ti/ Au (50 nm/200 nm) metal wiring layer, including metal neural electrode array, was deposited on parylene film using an electron beam evaporator (ED-1600, SANVAC Co., Ltd.). The array consists of 64 Ti/Au metal electrodes with an area of 80 × 80 μm^2 in a 32 (300 μm pitch) × 2 (400 or 800 μm pitch) configuration. The interconnected metal wiring layer was covered with 1 μm thick parylene film. A focal area of parylene was removed by CF_4 and O_2 plasma gas etching to form apertures on the Ti/Au electrode with specific and the device geometry (configuration) (RIE-200NL, Samco Inc.). Finally, the electrode array was mounted on a printed circuit board (PCB) with a design of 15.5 mm × 14.3 mm using flip chip bonder (M90, HiSOL, Inc.). The cross-section of the electrode array, which is placed on cerebral cortex, is shown in Fig. 1b

2.2. Animals

All animal procedures were approved by the Animal Care and Use Committee of Dokkyo Medical University and carried out in accordance with the guidelines of the National Institutes of Health. Native male mice C57BL6/J (Japan SLC, Inc., Shizuoka, Japan) were used at 3-6 months of

age. All mice were maintained on a 12 h light/dark cycle (lights on 7:00 am–7:00 pm) at 24 ± 3 °C and 55 ± 5% humidity, had ad libitum access to food and water, and were housed in a cage with littermates until surgery.

2.3. Surgical implantation of the flexible μECoG sheet

Male mice (n = 5, 31.1 ± 2.1 g) were implanted with μECoG arrays in the left cranial hemisphere. During surgery, mice were anesthetized with 0.75 mg/kg medetomidine hydrochloride, 4.0 mg/kg midazolam, and 5.0 mg/kg butorphanol tartrate for recordings under awake conditions, or urethane (1.2 g/kg) for recordings under anesthetized conditions. Mice were placed into a stereotaxic frame (Narishige, Tokyo, Japan) and on a heating pad to maintain normal body temperature (37 ˚C; MK-900, Muromachi Kikai, or ATC-TY, Unique-Medical Inc., Tokyo, Japan) during surgery. An incision was made in the scalp along the midline of the brain. After exposing the skull, a tendon of temporalis muscle connecting to the edge of parietal bone was cut to secure a space to perform implantation of the μECoG array (Fig. 1c-j). Four stainless steel anchor screws (AN-3, Eicom, Kyoto, Japan) were attached to the skull for mechanical support; one screw was placed on the frontal bone and one on the parietal bone, while the remaining screws, which served as ground and reference, were inserted into the interparietal bone above cerebellum (Fig. 1d). Before the craniotomy, dental acrylic (UNIFAST III, GC Corporation, Tokyo, Japan) was placed on the edge of the exposed skull to affix

screws and to protect ground and reference wires (Fig. 1e). The skull was drilled into a rectangular shape from bregma to lambda on the anteroposterior axis and from the right parietal bone to the left squamosal bone on the mediolateral axis (Fig. 1f). The surgical procedures ensured preservation of the dura. The head-fixation plate was taped onto the PCB in order to affix it on the head after implantation of the μECoG sheet. A male header pin (TSW-105-20-T-S, DegiKey, USA) was attached to the frontal bone for a device holder, and the μECoG was soldered to secure the PCB onto the skull (Fig. 1g). The μECoG array was carefully inserted into the space between the brain and squamosal bone (Fig. 1h). Note the flexible ECoG sheet was placed on the dura mater. After implantation, the craniotomy site was covered by the parietal bone that was removed during craniotomy, and was embedded using dental acrylic (Fig. 1i). A head-fixation plate, temporarily supported with tape on the PCB, was attached on the head (Fig. 1j, dashed line). After the surgery, mice were placed into a home cage and on a heating pad to maintain body temperature until recordings. Recordings from awake mice were conducted at least 3 hours after the completion of surgery.

2.4 Behavioral task and recordings

Mice were head-fixed on the apparatus and placed in a sound attenuated chamber for the multisensory presentation task. An electrical fan provided background sound (50 dB) and ventilation. White LED was placed in front of the right eye, and odor and air tubes were placed in front of the nose

and whiskers, respectively. The controller for multisensory presentations was developed using custom programs (LabView, National Instruments, TX). The program pseudorandomly controlled the visual (Frequency, 10 Hz), somatosensory (Flow rate, 2.5 L/min), and odor (Flow rate, 1 L/min, 0.01% benzaldehyde diluted in mineral oil) stimuli for 3 sec with intertrial intervals (~10-20 sec) that lasted for 100 or 150 trials in the awake or in the anesthetized experiment, respectively (50 trials each stimulus).

LFP and event signals were recorded at a sampling rate of 20 kHz using the Open Ephys recording system (www.open-ephys.org). Data were downsampled to 1,250 Hz for analysis. Neural signals were amplified on the 64-Channel head stage (C3325, Intan Technologies, USA). To connect the μECoG device and the head stage, a custom-made adapter corresponding to both the flexible flat cable connector (39FVXS-RSM1-GAN-TF, J. S. T. MFG. Co., Ltd, Japan) on the device and the nano strip connectors on the head stage (C3315, Omnetics, USA) was used. Data were analyzed using MATLAB software (MathWorks, MI, USA). The stimulus-evoked LFP was obtained by averaging the LFPs against stimulus onset across trials. To identify sensory stimulus-evoked LFPs on active channels, we compared the peak LFP amplitudes between the before (-600 to 0 ms) and after (0 to 600 ms) stimulus for each electrode. To compare the LFP amplitude between the different electrodes or stimuli, we also used the peak LFP amplitudes for 0.6 sec after stimulus onset. The current source density (CSD) for a set of voltage traces obtained from a linear array of an electrode sheet was calculated

using a CSD function written by Timothy Olsen (2022) (https://www.mathworks.com/matlabcentral/fileexchange/69399-current-source-density-csd).

2.5 Histological analysis

After the μECoG implantation and recordings, mice were deeply anesthetized with 5% isoflurane and an overdose of pentobarbital solution, and then transcardially perfused with 0.9% saline. To check the position of the μECoG sheet, the head was cut, and the muscles surrounding the skull were removed using a bone rongeur. The skull was quickly covered in crushed dry ice for flash-freezing. The frozen skull was stored at -30 ℃ until use. To prepare sections including brain, skull, and the flexible μECoG sheet, we used a polyvinylidene chloride film and a modification of a previously described method (Kawamoto, 2003). The skulls were embedded in OCT compound at −20°C for at least 20 min before slicing in the cryostat. After reaching to the sampling coordinates, the coronal surface of the brain was covered by transfer film (Cryofilm type IIC(9), SECTION-LAB, Hiroshima, Japan) to avoid detaching the skull, brain, and μECoG sheet from samples. Samples were cut at 30 μm. Serial sections were placed on glass slides (Matsunami, Osaka, Japan) and stained with 4',6-diamidino-2-phenylindole (DAPI; D9542, Sigma-Aldrich, St. Louis, MO) for 5 min. Sections were rinsed by phosphate buffered saline for 3 min and allowed to dry for 20 min. The films containing the sections were flipped onto a drop of embedding agent (ProLong antifade reagents, Thermo Fisher

Scientific, USA) on a new glass slide and gently pushed with a finger to adhere them to the substrate. The redundant embedding agent was removed by filter paper, and the perimeter of the film was covered with manicure to prevent tissue drying. Sections were scanned using a BZ-X700 (Keyence, Osaka, Japan) with 4 × objective lens. The contrast and color balance of images scanned under bright field and UV light conditions were adjusted using Photoshop (CC, Adobe Inc., USA). The images were superimposed for analysis.

2.6. CT imaging

To visualize the position of the μECoG electrode array without removing the skull, we used CT scans (Cosumo Scan Fx, Rigaku Corp., Tokyo Japan). After recordings, mice were perfused with 0.9% saline as described under histological analysis. The PCB of the μECoG and header pin were removed from the head of mice, and the remaining ECoG sheet was bonded to the skull to avoid displacement of the electrode position. The CT data were obtained using the following parameters; tube voltage, 90 kV; tube current, 88 μA; exposure time, 2 min; and resolution 20 μm isotropic.

2.7. Statistics

Statical analysis was performed using MATLAB software. Comparison of data between two groups were performed using the Student's *t*-test (paired), the Wilcoxon signed rank test (paired), and

the Wilcoxon rank-sum test (unpaired). Comparison of data between three groups were constructed using a one-way repeated measures ANOVA or the Friedman test (without assuming normal distribution and homogeneity of variances). The level of statistical significance for variables was set at *$p < 0.05$, **$p < 0.01$, ***$p < 0.001$, †$p < 0.05$, †††$p < 0.001$. All statical tests were two-sided.

3. Results

3.1. Device fabrication

The thickness of the film is an important factor of stiffness for proper device insertion into the epidural space between the temporal cortex and skull. Devices with different thicknesses were fabricated to understand the effect of parylene thickness on the self-supporting characteristics. The parylene thicknesses T_p of the devices prepared in this study were 7, 13 and 23 μm. Fig. 2a shows photographs of the neural electrode array device with different thicknesses, including optical micrographs of the electrode array. The thin device was curled up owing to strain caused by the thermal expansion coefficient between metal and parylene. As increased thickness of the film results in increased bending stiffness, the thick device was not as curled, but resulted in more robust self-supporting characteristics relative to the thin device. The bending stiffness S of the parylene film without metal can be expressed as

$$S = \frac{1}{12} E_p b T_p^3 \qquad (1)$$

where E_p, and b are the Young's modulus (E_p = 2.78 GPa) and the width (b = 3.1 mm) of parylene film, respectively. It can be seen that S increases rapidly with increasing the T_p. The actual device contains 64 channel Ti/Au metal wiring layer with a high Young's modulus, which affects S. The structured-corrected S was theoretically calculated based on a previous report (Kim et al., 2010). Fig. 2b shows the calculated bending stiffness of the device with and without the metal wiring layer as a function of the parylene thickness. The S of the device with the metal layer is ~1.3-1.4 times higher than that of the device without the metal layer. To determine the optimal device design, the thickness and width for parylene, and also the thickness, width, and number of metal wire channels were key factors. Fig. 2c shows the frequency dependence of impedance from a representative neural electrode. All the electrodes showed almost the same characteristics. The impedances at 1 kHz were approximately 0.5 MΩ.

3.2. Histological validation of μECoG sheet position

To examine whether the 23 μm flexible μECoG sheet appropriately reaches to the ventral parts of temporal cortex along the curved surface of mouse cerebral cortex, we histologically validated the position of the μECoG sheet by using adhesive transfer film to prevent the samples from separating (Kawamoto and Shimizu, 2000) (Fig. 3a, see methods). Briefly, we prepared sections including brain, skull, and μECoG sheet and took microscopic images under conditions for bright field and DAPI

(nuclear staining). The results showed that the μECoG sheet was situated along the surface of cerebral cortex (Fig. 3a, black arrows), and the tip of the μECoG sheet approached the piriform cortex, which is the most ventral part of the temporal cortex (Fig. 3a, red arrows). In addition, comparisons between ipsilateral and contralateral hemispheres showed no obvious damage in either the dorsal or ventral parts of the cerebral cortex that may have resulted from the surgical procedures required for device insertion (Fig. 3b-d).

3.3. LFP Recordings in an awake mouse

First, we tested whether the μECoG electrode arrays, implanted onto the temporal cortex by our surgical methods, can monitor LFPs from a broad cortical area of an awake and head-fixed mouse, while also recording sensory stimulus-evoked potentials. Half of the electrodes on the μECoG sheet were inserted into the space between the temporal cortex and skull, and the remaining electrodes were situated on the parietal part of cortex (Fig. 4a). The location of the μECoG sheet in the temporal cortex was confirmed by a CT imaging after the experiment, and the tip of the sheet reached to the most ventral part of the temporal cortex (Fig. 4b), which is comparable with the histological assessment (Fig. 3a). Histological and CT assessments indicated that our μECoG electrodes were placed on parietal to temporal cortices, including the barrel and piriform cortices. Under this condition, we recorded LFPs with the μECoG electrode arrays (Fig. 4c) along with the dorsoventral axis of the cortex.

Representative LFPs recorded by successive thirty-two electrodes are shown in Fig. 4d. The recording condition was reliably maintained for at least 3 hours under the acute experimental condition.

Next, we conducted a sensory cue-presentation task to record cortical potentials responding to sensory stimuli (Fig. 4e). In this experiment, we applied a tactile stimulus to the vibrissa in the form of mild air flow because the ECoG electrode arrays easily target the barrel cortex. The visual stimulus was used as a control stimulus as no electrodes were placed on the visual cortex, which is located in a more posterior region than the barrel cortex. Sensory stimuli were pseudorandomly presented to the mouse every ~10–20 sec. The tactile stimulus induced strong tactile-evoked LFPs in the electrodes placed over the parietal region of the cortex, whereas the visual stimulus did not induce changes in the LFPs recorded from all channels (Fig. 4f). To examine the response characteristics to sensory stimuli on the same channel or between separated channels, we compared the amplitudes of maximal responses of another sensory stimulus and different electrodes to the tactile stimulus. We confirmed that channel 58 showed the maximal change in tactile stimulus-evoked LFP (Fig. 4g, Wilcoxon signed-rank test, $Z = 6.009$, $p < 0.001$, for comparison with baseline amplitudes), which was significantly higher than that of visual stimulus-evoked LFPs (Fig. 4g, Wilcoxon signed-rank test, $Z = 6.087$, $p < 0.001$). Moreover, we confirmed that the peak amplitudes of tactile stimulus-evoked LFP at channel 58 was significantly higher than that of channel 33 (Fig. 4h, Wilcoxon rank-sum test, $Z = 5.112$, $p < 0.001$), the most ventral electrode. We also characterized the origin of sensory-evoked LFPs by CSD

analysis from μECoG electrodes equally spaced on parietal to temporal cortices. The position of a robust sink-source dipole was identified at channels surrounding channel 58 (Fig. 4i).

3.4. LFP recordings in anesthetized mice

We tested whether the μECoG electrode array covering the parietal to temporal cortices can monitor cortical activity corresponding to multiple sensory stimuli. In this experiment, we conducted a sensory cue-presentation task that added an odor stimulus to the previous task that used tactile and visual stimuli (Fig. 5a). The neural recordings were carried out under urethane anesthesia because sniffing or chowing behaviors were frequently observed in mice not habituated to the novel odors of the task environments. As shown in Fig. 4a, approximately half of the electrode array on the μECoG sheet were inserted into the epidural space between the temporal cortex and skull, while the other electrodes were placed on the parietal cortex (Fig. 5b).

Representative LFP data were recorded by the μECoG electrode arrays from a wide area of cerebral cortex. Before the sensory cue-presentation task, we confirmed the presence of cortical LFPs from parietal to temporal cortices under anesthetized conditions (Fig. 5c, representative LFP). In the sensory cue-presentation task, tactile, odor, and visual stimuli were presented to the mouse pseudorandomly 50 times for each sensory modality (150 times total), every ~10-20 sec. We observed clear tactile and odor stimulus-evoked LFPs from electrodes located on both parietal (Ch. 58 and 62)

and temporal (Ch. 33 and 37) cortices, respectively (Fig. 5c, averaged LFP). Sensory stimulus-evoked LFPs were not observed from the electrode placed on the middle position of the recording areas along the dorsoventral axis (Ch. 15). We next measured the maximal amplitudes of the sensory stimulus-evoked LFP responses to the tactile, odor, and visual stimuli (50 trials each) in four mice. In channels placed on the parietal cortex, the tactile stimulus induced significantly higher evoked LFP amplitudes relative to the baseline amplitudes that were recorded just before the stimulus onset (Fig. 5d, Wilcoxon signed-rank test, $Z = 4.609$, $p < 0.001$ for Mouse #1, $Z = 3.595$, $p < 0.001$ for Mouse #2, $Z = 6.042$, $p < 0.001$ for Mouse #3, $Z = 4.581$, $p < 0.001$ for Mouse #4). The tactile stimulus did not result in higher evoked LFP amplitudes than visual and odor stimuli in the same channels in one mouse (Fig. 5d; Friedman test, $\chi^2 = 1.12$, $p = 0.571$, for Mouse #1). In another mouse, the amplitudes evoked by the tactile stimulus were significantly higher than those evoked by the visual stimulus (Fig. 5d; one-way repeated ANOVA, $F(2,147) = 4.86$, $p < 0.01$, *post hoc* Tukey–Kramer test, tactile vs. odor, $p = 0.805$, tactile vs. visual, $p < 0.01$, odor vs. visual, $p = 0.052$, Mouse #2). In the remaining two mice, the tactile stimulus evoked higher amplitudes relative to the other stimuli (Fig. 5d; Friedman test, $\chi^2 = 39.04$, $p < 0.001$, *post hoc* Tukey–Kramer test, tactile vs. odor, $p < 0.001$, tactile vs. visual, $p < 0.001$, odor vs. visual, $p = 0.916$ for Mouse #3; $\chi^2 = 14.68$, $p < 0.001$, *post hoc* Tukey–Kramer test, tactile vs. odor, $p < 0.01$, tactile vs. visual, $p < 0.01$, odor vs. visual, $p = 0.916$ for Mouse #4). The amplitudes of odor stimulus-evoked LFP recordings from channels located on the ventral parts of the temporal cortex

were significantly higher than the baseline amplitude in three mice, but not in one mouse (Mouse #3) (Fig. 5e; Wilcoxon signed-rank test, $Z = 3.464$, $p < 0.001$ for Mouse #1, $Z = 5.146$, $p < 0.001$ for Mouse #2; paired Student's *t*-test, $t_{(49)} = 2.471$, $p < 0.05$ for Mouse #4). In the three mice, the odor-evoked LFP amplitudes tended to be higher than other stimuli-evoked LFP amplitudes (Fig. 5e). Two of the mice showed that the odor stimulus-evoked amplitudes were larger than either the visual or tactile-evoked LFP amplitudes (Fig. 5e; Friedman test, $\chi^2 = 8.32$, $p < 0.05$, *post hoc* Tukey–Kramer test, tactile vs. odor, $p = 0.112$, tactile vs. visual, $p = 0.703$, odor vs. visual, $p < 0.05$ for Mouse #1; $\chi^2 = 6.28$, $p < 0.05$, *post hoc* Tukey–Kramer test, tactile vs. odor, $p < 0.05$, tactile vs. visual, $p = 0.514$, odor vs. visual, $p = 0.341$ for Mouse #4). On the other hand, the remaining one mouse exhibited odor stimulus-evoked amplitudes were larger than either the visual or tactile-evoked LFP amplitudes. (Fig. 5e; Friedman test, $\chi^2 = 20.32$, $p < 0.001$, *post hoc* Tukey–Kramer test, tactile vs. odor, $p < 0.001$, tactile vs. visual, $p = 0.978$, odor vs. visual, $p < 0.001$ for Mouse #2).

4. Discussions

EEG and ECoG recordings in humans and non-human primates are used to record neural activity from a wide area of cerebral cortex, including the temporal lobe, with high temporal and spatial resolution (Kaneko et al., 2022; Wang et al., 2009). However, there are no techniques to record from the temporal cortex using these techniques in rodents. Such a techniques would provide a powerful

tool for neuroscience. Here, we describe the development of a novel μECoG electrode array, including surgical techniques for implanting the device into the mouse temporal cortex. We also confirm the availability of large-scale LFP recordings from the novel μECoG electrode array. We show that array thickness is a key factor for the usefulness of parylene-based electrodes. Appropriate stiffness of the μECoG sheet-shaped electrode allowed its insertion into the space between the skull and brain surface, while minimizing the invasiveness of the arrays on the mouse cerebral cortex. In addition, the device could reliably assess sensory stimulus-evoked LFPs from the multiple recording sites covering the somatosensory and olfactory cortex both in awake and anesthetized mice. These techniques are suitable for understanding mechanisms relevant to cognitive functions and pathological conditions in which inter-regional network activities are involved.

Tissue penetrating neural electrode arrays are the primary method used for in vivo neuronal recordings in rats and mice. However, damages to brain tissue or dura mater cannot be avoided, and glial scar formation can occur around electrode arrays, leading to quality degradation of neural signals (Kotov et al., 2009). By contrast, sheet-shaped ECoG electrode arrays are less invasive than penetrating electrode arrays. Several groups have developed insertable devices that implant onto the brain surface, beneath the skull (Hollenberg et al., 2006; Jeong et al., 2021; Park et al., 2016; Yeager et al., 2008). Although these techniques enabled neural recordings from a relatively wide area of the cerebral cortex without penetrating the brain and with little surgery-related tissue trauma, the recording

areas were limited to the dorsal parts of cerebral cortex in rodents. Our μECoG sheet overcomes this limitation by expanding the area of cortical recordings to other areas. Using CT imaging and histological methods, we confirmed that placement of the μECoG sheet-shaped array covered the area from the somatosensory cortex to the piriform cortex (Franklin and Paxinos, 2007) without structural damage to the cortical surface. In addition, odor stimulus-evoked LFPs were observed from electrodes placed on the tip of the array. These results strongly demonstrate that our μECoG can record from a wider area of the mouse cerebral cortex than existing ECoG methods., This novel μECoG method may shed light on neural network interactions between the parietal and temporal cortex in mice.

In this study, we characterized the performance of our μECoG device under awake and anesthetized conditions. The next step would be to assess the usefulness of the device under chronic conditions. The μECoG device was fabricated using parylene, which is a biocompatible material. Previous studies have indicated that parylene-based μECoG devices can maintain electric impedance and the quality of chronic recordings for up to two weeks (Toda et al., 2011). Additionally, our surgical methods enabled implantation of the electrode array without structural damage to the dura matter or the layered tissue structures of the cerebral cortex (Fig. 3b-d), despite the wide-area craniotomy needed for electrode placement (Fig. 1g, 4a, and 5b). Our results are consistent with those of a previous study describing a methodology for implanting an μECoG device into the space between the brain surface and skull (Park et al., 2016). Together, the characteristics of our device and surgical methods suggest

that they can be used in chronic applications. On the other hand, chronically implanted μECoG devices can cause micro-hematomas and result in opaque connective tissue, which can effect normal cortical activity (Schendel et al., 2013). Further studies should investigate whether the signal quality is maintained several weeks after implanting the μECoG device using our novel methodology.

ECoG and μECoG techniques can be employed in humans, non-human primates, and rodents using a similar methodology (Kaneko et al., 2022; Khodagholy et al., 2015; Wang et al., 2009), thus providing physiological data that can be compared across species. However, the measurement area of current μECoG techniques in mice is limited to the relatively small cortical surface area, and currently does not include the temporal and occipital cortex, which are easily addressed in humans and non-human primates. The μECoG device developed here is insertable into the most ventral parts of the epidural space and makes it possible to record cortical activity from the dorsal to ventral cortices of mice, which has previously been difficult to achieve. Our approach extends the possibility of comparing features of ECoG recordings between mouse and human and non-human primates. Therefore, our μECoG device and methodologies could promote translational research by applying them to rodent models of various pathologies. Possibilities include the combination of μECoG recordings with optogenetics to investigate the causes of diseases. In the future, the integration of these genetical tools and large-scale μECoG recordings may help to further elucidate the mechanisms underpinning neuropsychiatric disorders.

5. Conclusion

In this study, we developed a 64-channel μECoG device covering the parietal to temporal cortex in mice. The novel surgical procedures enable device placement on the piriform cortex, which is the most ventral part of the mouse cerebral cortex. The device recorded stimulus-evoked potential across multiple sensory areas of cerebral cortex along the dorsal-ventral axis. This system will provide opportunities to investigate physiological functions from wider areas of the mouse cerebral cortex than those of existing ECoG techniques.

Acknowledgments

We thank the Research Center for Laboratory Animals, Dokkyo Medical University for animal maintenance, the Center for Research Collaboration and Support, Dokkyo Medical University for allowing to use the BZ-X700 fluorescence microscope, and S. Fujiki, T. Hikima, and all members of Division for Memory and Cognitive Function, Dokkyo Medical University for valuable discussions.

Funding

This work was supported by the JSPS KAKENHI (19K20074, 19J01997, 21K11556, and 21H05244) (to S.S.), the Tochigi Industrial Promotion Center (the Grant-in-Aid for World-Class Technological Research and Development) (to S.S.), the Nakatomi Foundation (to S.S.), the Dokkyo Medical University, Investigator-Initiated Research Grant (2020-3) (to S.S.), the Dokkyo Medical University, Project Research Grant (2021-06) (to S.S.), the Dokkyo International Medical Education and Research Foundation (to S.S. and N.O.), the JST PRESTO (JPMJPR1885) (to H.S.), the Casio Science Promotion Foundation (to H.S.), the Toyoaki Scholarship Foundation (to H.S.), the Foundation of Public Interest of Tatematsu (to H.S.), the Research Foundation for Opto-Science and Technology (to H.S. and N.O.), the Naito Foundation (to N.O.), the Astellas Foundation for Research on Metabolic Disorders (to N.O.), and the Takeda Science Foundation (to N.O.). The authors declare no conflicts of interest.

Author contributions

S.S., H.S., and N.O. conceived the project. O.F. and M.O. evaluated the characteristics of the μECoG device. S.S. and Y.S. performed the animal experiments. S.S. analyzed the data. M.I. and S.N. performed the histological experiments. R.K. and S.T. performed the fabrications and its measurements for the μECoG device. H.M. and K.M. supported the developments for behavioral

apparatus and systems. F.S. and K.H. scanned CT imaging. S.S., R.K., H.S., and N.O. wrote the manuscript.

References

Baverstock H, Jeffery NS, Cobb SN. The morphology of the mouse masticatory musculature. Journal of Anatomy, 2013; 223: 46-60.

Choi JH, Koch KP, Poppendieck W, Lee M, Shin H-S. High resolution electroencephalography in freely moving mice. Journal of neurophysiology, 2010; 104: 1825-34.

Franklin K, Paxinos G. The Mouse Brain in Stereotaxic Coordinates 3rd edn (New York: Academic). 2007.

Gilad A, Helmchen F. Spatiotemporal refinement of signal flow through association cortex during learning. Nature communications, 2020; 11: 1-14.

Hollenberg BA, Richards CD, Richards R, Bahr DF, Rector DM. A MEMS fabricated flexible electrode array for recording surface field potentials. Journal of neuroscience methods, 2006; 153: 147-53.

Jeong U-J, Lee J, Chou N, Kim K, Shin H, Chae U, Yu H-Y, Cho I-J. A minimally invasive flexible electrode array for simultaneous recording of ECoG signals from multiple brain regions. Lab on a Chip, 2021; 21: 2383-97.

Kaiju T, Doi K, Yokota M, Watanabe K, Inoue M, Ando H, Takahashi K, Yoshida F, Hirata M, Suzuki T. High spatiotemporal resolution ECoG recording of somatosensory evoked potentials with flexible micro-electrode arrays. Frontiers in neural circuits, 2017; 11: 20.

Kaneko T, Komatsu M, Yamamori T, Ichinohe N, Okano H. Cortical neural dynamics unveil the rhythm of natural visual behavior in marmosets. Communications biology, 2022; 5: 1-13.

Kawamoto T. Use of a new adhesive film for the preparation of multi-purpose fresh-frozen sections from hard tissues, whole-animals, insects and plants. Archives of histology and cytology, 2003; 66: 123-43.

Kawamoto T, Shimizu M. A method for preparing 2-to 50-µm-thick fresh-frozen sections of large samples and undecalcified hard tissues. Histochemistry and cell biology, 2000; 113: 331-9.

Khodagholy D, Gelinas JN, Buzsaki G. Learning-enhanced coupling between ripple oscillations in association cortices and hippocampus. Science, 2017; 358: 369-72.

Khodagholy D, Gelinas JN, Thesen T, Doyle W, Devinsky O, Malliaras GG, Buzsáki G. NeuroGrid: recording action potentials from the surface of the brain. Nature neuroscience, 2015; 18: 310-5.

Kim D-H, Viventi J, Amsden JJ, Xiao J, Vigeland L, Kim Y-S, Blanco JA, Panilaitis B, Frechette ES, Contreras D. Dissolvable films of silk fibroin for ultrathin conformal bio-integrated electronics. Nature materials, 2010; 9: 511-7.

Kimura R, Saiki A, Fujiwara-Tsukamoto Y, Ohkubo F, Kitamura K, Matsuzaki M, Sakai Y, Isomura Y. Reinforcing operandum: rapid and reliable learning of skilled forelimb movements by head-fixed rodents. Journal of neurophysiology, 2012; 108: 1781-92.

Konerding W, Froriep U, Kral A, Baumhoff P. New thin-film surface electrode array enables brain

mapping with high spatial acuity in rodents. Scientific reports, 2018; 8: 1-14.

Kotov NA, Winter JO, Clements IP, Jan E, Timko BP, Campidelli S, Pathak S, Mazzatenta A, Lieber CM, Prato M. Nanomaterials for neural interfaces. Advanced Materials, 2009; 21: 3970-4004.

Kramer MA, Cash SS. Epilepsy as a disorder of cortical network organization. The Neuroscientist, 2012; 18: 360-72.

Lee JY, Jun H, Soma S, Nakazono T, Shiraiwa K, Dasgupta A, Nakagawa T, Xie JL, Chavez J, Romo R. Dopamine facilitates associative memory encoding in the entorhinal cortex. Nature, 2021; 598: 321-6.

Li R, Nguyen T, Potter T, Zhang Y. Dynamic cortical connectivity alterations associated with Alzheimer's disease: An EEG and fNIRS integration study. NeuroImage: Clinical, 2019; 21: 101622.

Park AH, Lee SH, Lee C, Kim J, Lee HE, Paik S-B, Lee KJ, Kim D. Optogenetic mapping of functional connectivity in freely moving mice via insertable wrapping electrode array beneath the skull. ACS nano, 2016; 10: 2791-802.

Rogers-Carter MM, Varela JA, Gribbons KB, Pierce AF, McGoey MT, Ritchey M, Christianson JP. Insular cortex mediates approach and avoidance responses to social affective stimuli. Nature neuroscience, 2018; 21: 404-14.

Schendel AA, Thongpang S, Brodnick SK, Richner TJ, Lindevig BD, Krugner-Higby L, Williams JC. A cranial window imaging method for monitoring vascular growth around chronically implanted

micro-ECoG devices. Journal of neuroscience methods, 2013; 218: 121-30.

Sheybani L, Birot G, Contestabile A, Seeck M, Kiss JZ, Schaller K, Michel CM, Quairiaux C. Electrophysiological evidence for the development of a self-sustained large-scale epileptic network in the kainate mouse model of temporal lobe epilepsy. Journal of Neuroscience, 2018; 38: 3776-91.

Toda H, Suzuki T, Sawahata H, Majima K, Kamitani Y, Hasegawa I. Simultaneous recording of ECoG and intracortical neuronal activity using a flexible multichannel electrode-mesh in visual cortex. Neuroimage, 2011; 54: 203-12.

Uhlhaas PJ, Singer W. Abnormal neural oscillations and synchrony in schizophrenia. Nature reviews neuroscience, 2010; 11: 100-13.

Vázquez-Guardado A, Yang Y, Bandodkar AJ, Rogers JA. Recent advances in neurotechnologies with broad potential for neuroscience research. Nature neuroscience, 2020; 23: 1522-36.

Wang D, Liu P, Mao X, Zhou Z, Cao T, Xu J, Sun C, Li A. Task-demand-dependent neural representation of odor information in the olfactory bulb and posterior piriform cortex. Journal of Neuroscience, 2019; 39: 10002-18.

Wang W, Degenhart AD, Collinger JL, Vinjamuri R, Sudre GP, Adelson PD, Holder DL, Leuthardt EC, Moran DW, Boninger ML. Human motor cortical activity recorded with Micro-ECoG electrodes, during individual finger movements. 2009 Annual International Conference of the IEEE Engineering in Medicine and Biology Society. IEEE, 2009: 586-9.

Yeager JD, Phillips DJ, Rector DM, Bahr DF. Characterization of flexible ECoG electrode arrays for chronic recording in awake rats. Journal of neuroscience methods, 2008; 173: 279-85.

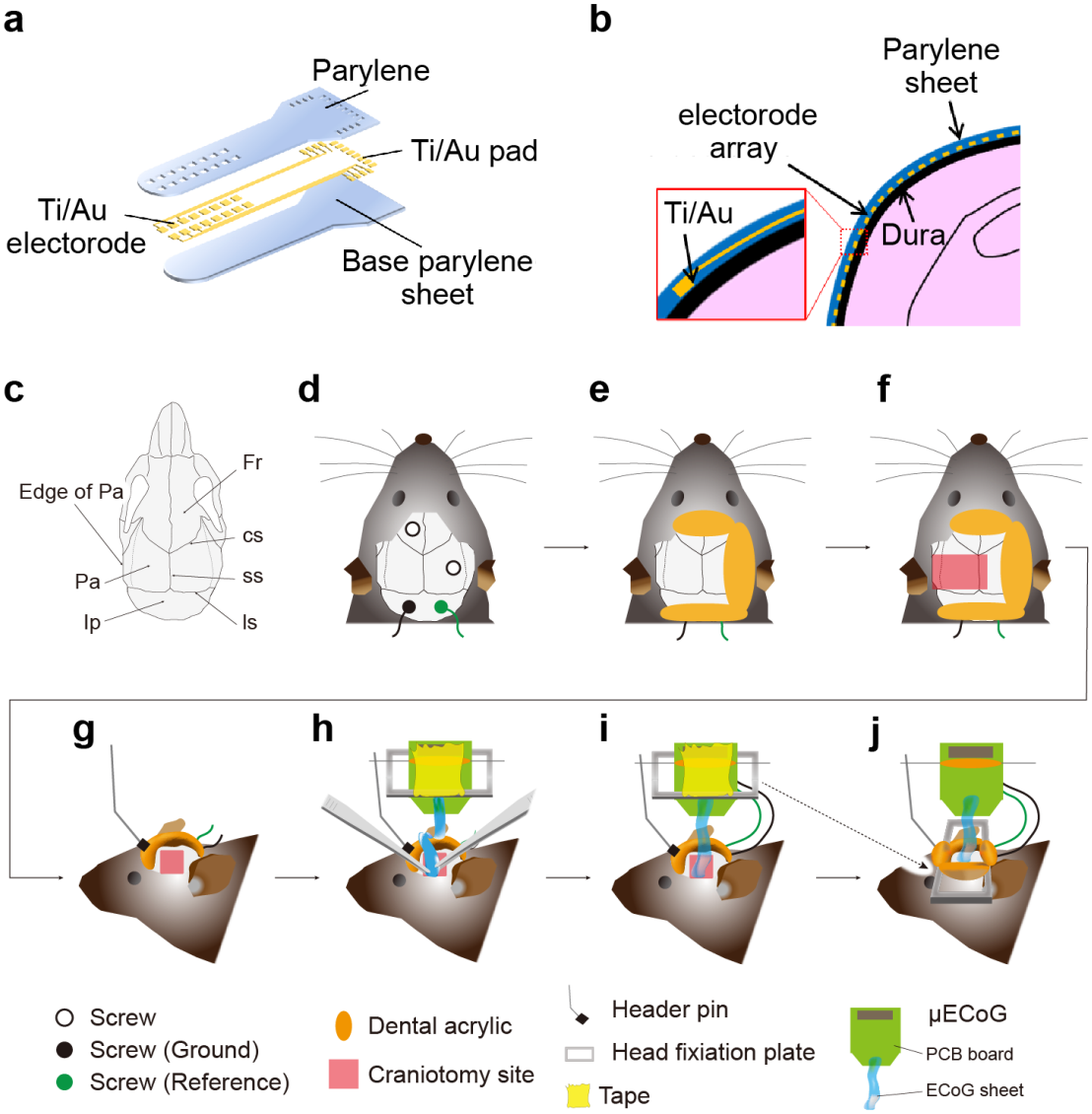

Fig. 1. Surgical procedures for the placement of the sheet-shaped μECoG device. (a) A schematic of the device showing its various components. (b) Schematic representation of a cross-section of the neural electrode array device placed on the cerebral cortex. (c) The cranial sutures in the dorsal view, Fr, Frontal bone; IP, Interparietal bone; Pa, parietal bone; cs, coronal suture; ss, sagittal suture; ls, lambdoid suture; edge of Pa, the edge of parietal bone connecting the temporalis muscle. (d-j) Schematic representations of the surgical procedures for inserting the μECoG electrode array into the

space between the brain and skull.

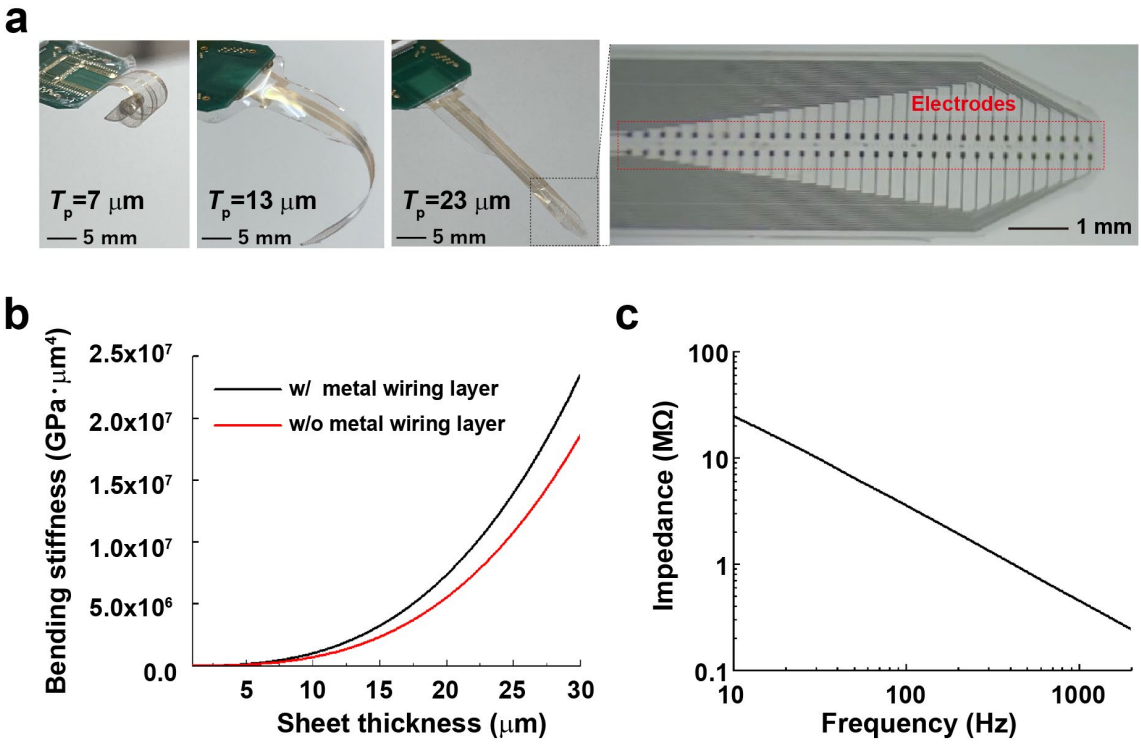

Fig. 2. Bending stiffness of the sheet-shaped μECoG device. (a) Photographs of a μECoG sheet with different parylene thicknesses of 7, 13, 23 μm and an optical microscope image of a sheet with arranged neural electrodes (Ti/Au). While the 7 μm thick sheet strongly curls, the 23 μm thick sheet has high self-supporting characteristics. (b) Calculated bending stiffness of the device with and without the metal wiring layer as a function of the parylene thickness. (c) Frequency dependence of impedance of the representative neural electrode. The impedance at 1 kHz was approximately 0.5 MΩ.

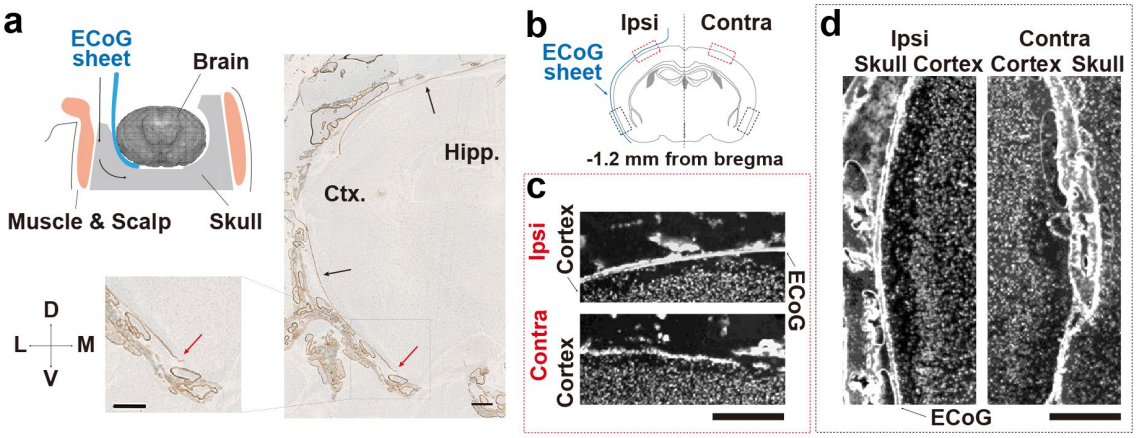

Fig. 3. Histological validation of the μECoG sheet position. (a) A schematic of the position of the μECoG sheet placed on the brain surface (upper left). Superimposed microscopic images of bright field and DAPI staining (right and lower left). Black arrows indicate the μECoG sheet on the brain surface. The insets show enlargements of the dashed rectangle. Red arrows indicate the tip of the μECoG sheet. Scale bars: 100 μm. Ctx, cortex; Hipp, hippocampus; D, dorsal; M, medial; V, ventral; L, lateral. (b-d) Comparison of cortical structure between the μECoG sheet-inserted hemisphere (ipsi-lateral side) and opposite hemisphere (contralateral side). Ipsi, ipsilateral; Contra, contralateral. (b) Schematic drawing of a coronal view of the mouse brain; black and red dashed rectangles indicate the parietal (c) and temporal cortex (d), respectively. Scale bars: 500 μm.

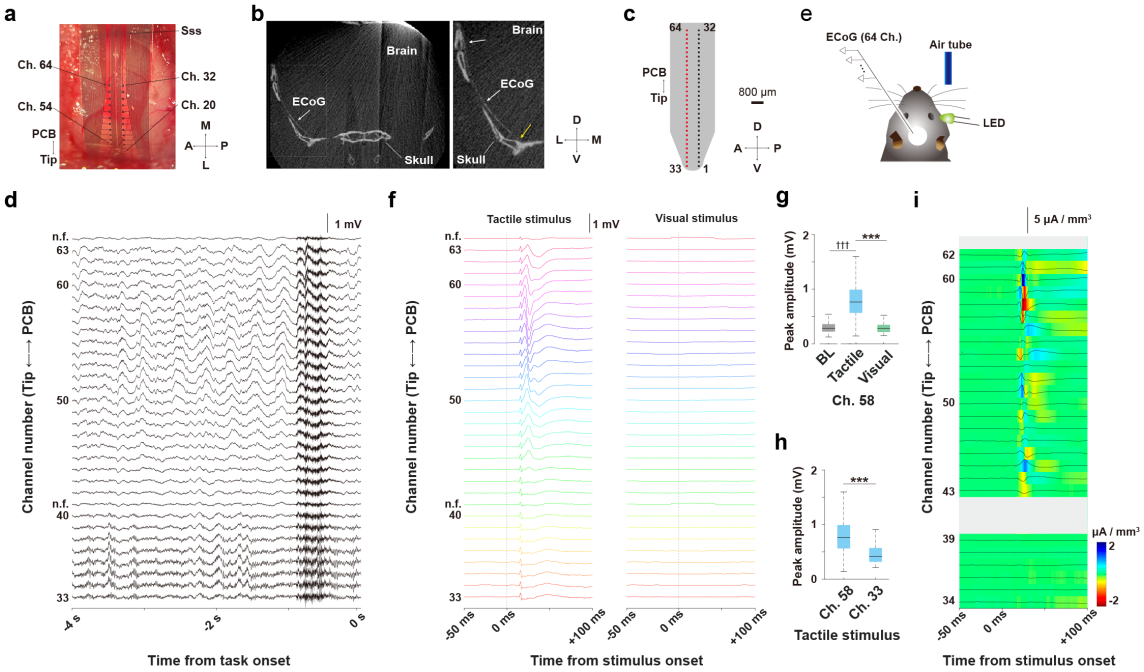

Fig. 4. LFP Recordings by the μEcoG sheet electrode in an awake mouse (a) Dorsal view of the μEcoG electrode array placed on the parietal cortex. M, medial; L, lateral; A, anterior; P, posterior; Ch., channel of electrode; Sss, superior sagittal sinus. (b) The position of the μEcoG sheet placed on the brain surface as revealed by CT scanning. White arrows indicate the μEcoG sheet placed on space between the brain and skull. The enlarged image (right) shows the tip of μEcoG sheet in the brain (yellow arrow). D, dorsal; V, ventral; M, medial; L, lateral. (c) The 64-channel μECoG electrode array. Numbers are the channel IDs of the electrode. Red rectangles indicate the thirty-two successive electrodes that recorded representative LFPs along the dorsoventral axis of the cortex. D, dorsal; V, ventral; A, anterior; P, posterior. (d) Representative LFPs before the sensory presentation task. Numbers indicate channels of the electrode corresponding to (c). n.f., not function. (e) Schematic drawing of the sensory presentation task and recordings in a head-fixed mouse. (f) Average sensory-

evoked LFPs. (g) Averaged peak LFP amplitudes in the same channels elicited by different stimuli. BL, baseline. (h) Averaged peak LFP amplitudes in different channels elicited by the same stimulus. (i) The current source density map calculated from the averaged tactile-evoked LFPs in (f). The central lines and edges of the boxes indicates the median and quartiles, respectively, and whiskers extend to the maximum and minimum. ***$P < 0.001$. ††† < 0.001 vs. baseline amplitude.

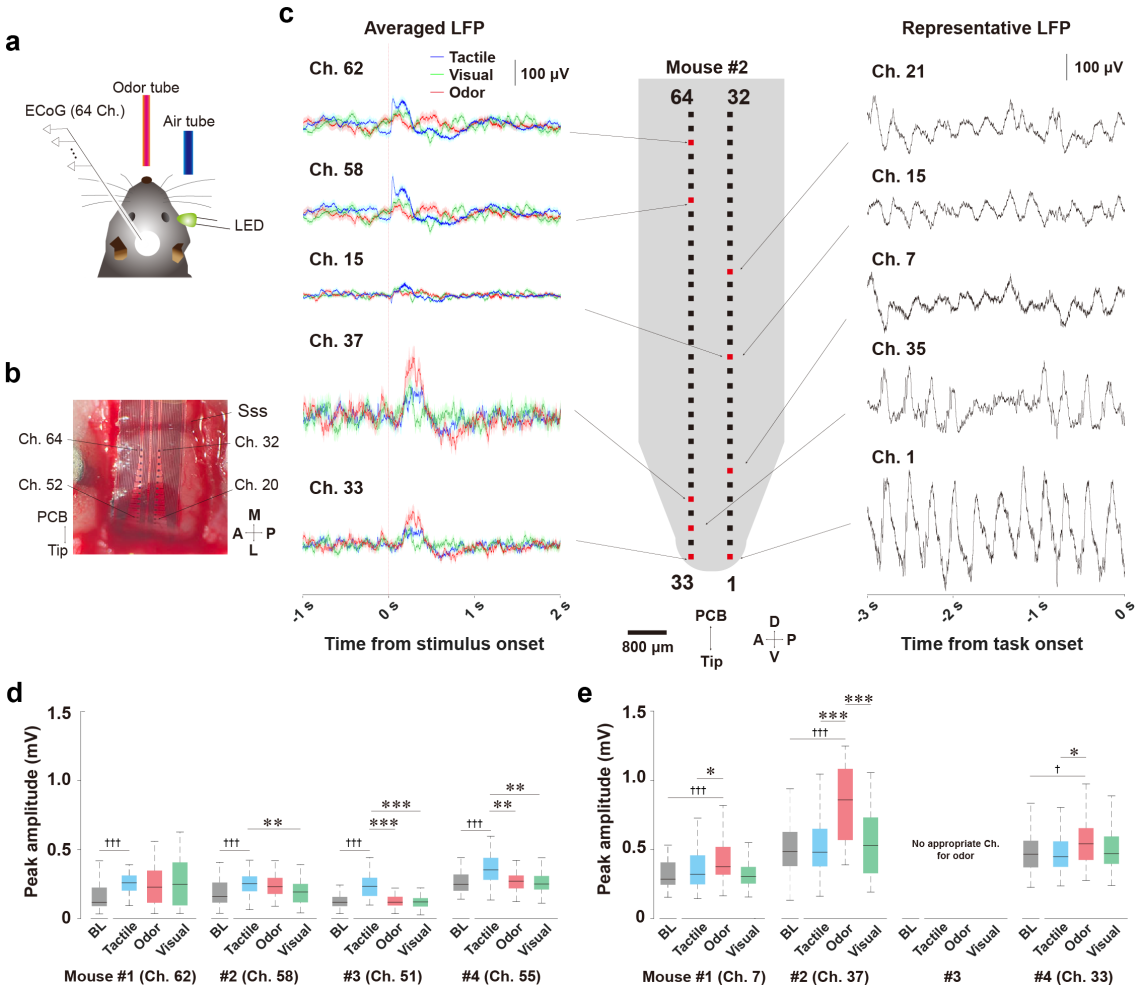

Fig. 5. The μECoG electrode can monitor cortical activities in response to multiple sensory stimuli. (a) Schematic drawing of the sensory presentation task and recordings in a head-fixed mouse. (b) Dorsal view of the μECoG electrode array on the parietal cortex. M, medial; L, lateral; A, anterior; P, posterior; Ch., channel of electrode; Sss, superior sagittal sinus. (c) The 64-channel μECoG electrode array and LFPs at start of the task (representative LFP) or on task (averaged LFP) in a mouse. LFPs corresponding to the tactile, visual, and odor stimuli are indicated as blue, green, and red line, respectively. Shadows indicate SEM. D, dorsal; V, ventral; A, anterior; P, posterior. (d) Averaged peak LFP amplitudes recorded by the channels in which the maximal change was observed for the tactile

stimulus. BL, baseline. (e) Averaged peak LFP amplitudes recorded by the channels in which the maximal change was observed for the odor stimulus. There are no channels showing the significant difference between odor stimulus-evoked and baseline LFP amplitudes in the #3 mouse. The central lines and edges of the boxes indicate the median and quartiles, respectively, and whiskers extend to the maximum and minimum with outliers excluded. *$P > 0.05$, ***$P < 0.001$ vs. each stimulus. †$P > 0.05$, ††† < 0.001 vs. baseline amplitude.